PNAS NEXUS

PNAS Nexus, 2025, 4, pgaf157
https://doi.org/10.1093/pnasnexus/pgaf157
Advance access publication 17 May 2025
Research Report

Molecular choreography of sludge extracellular polymeric substances—From biomolecule identification to energetics and assembly dynamics

Sainan Peng[a,b], Zhiyue Wang[c,d,*], Jing Ai[e], Lanfeng Li[e], Hao Zhou[e], Yu Zhang[e], Guiying Liao[a], Dongsheng Wang[f], Bing-Jie Ni[b], Guo-Ping Sheng[g], Chengzhi Hu[h,i] and Weijun Zhang[e,j,*]

[a]Faculty Materials Science and Chemistry, China University of Geosciences, Wuhan 430074, Hubei, China
[b]School of Civil and Environmental Engineering, The University of New South Wales, Sydney, NSW 2052, Australia
[c]Department of Civil and Environmental Engineering, University of Hawai'i at Mānoa, USA, Honolulu, HI 96822-2217, USA
[d]Water Resources Research Center, University of Hawai'i at Mānoa, Honolulu, HI 96822-2217, USA
[e]School of Environmental Studies, China University of Geosciences, Wuhan 430074, Hubei, China
[f]College of Environmental and Resource Sciences, Zhejiang University, Hangzhou 310058, Zhejiang, China
[g]CAS Key Laboratory of Urban Pollutant Conversion, Department of Environmental Science and Engineering, University of Science and Technology of China, Hefei 230026, China
[h]State Key Laboratory of Environmental Aquatic Chemistry, Research Center for Eco-Environmental Sciences, Chinese Academy of Sciences, Beijing 100085, China
[i]University of Chinese Academy of Sciences, Beijing 100049, China
[j]National Engineering Research Center of Industrial Wastewater Detoxication and Resource Recovery, Research Center for Eco-Environmental Sciences, Chinese Academy of Sciences, Beijing 100085, China
*To whom correspondence should be addressed: Email: zhiyue@hawaii.edu, zhangweijun@cug.edu.cn
Edited By Levi Thompson

Abstract

Extracellular polymeric substances (EPS) shape the immediate environment for microbial survival and biofilm formation. Dynamic agglomeration of EPS dominates the formation kinetics and structural properties of activated sludge flocs as a consequence of biopolymer interactions across the wastewater treatment process. Current partial understanding and imprecise modeling of the structure hinder the comprehensive elucidation of the dynamic reorganization of clusters as component interactions change, causing a gap in the fundamental knowledge of EPS generation and functions. Here, biopolymer models of aerobic activated sludge and anaerobic digestion sludge (ADS) were constructed through molecular screening, and the dynamic landscape of EPS multicomponent clusters was then captured by an extensive set of molecular dynamics simulations. Biopolymer chains are assembled hierarchically driven by interactions between polar functional groups and stabilized by hydrogen bonding and van der Waals forces after several substates to obtain the final conformation. Electrostatic repulsion induced by carboxylic groups causes the rugged energy landscape of the process. Biopolymer molecular arrangement governed by polar interactions determines the nonuniform distribution of functional groups and characteristic regions, resulting in the microscopic heterogeneity of EPS clusters. The structure of alpha-helices enhances protein aggregation efficacy by facilitating more polar interactions compared with other residues. Meanwhile, the flexible branched structure and amphiphilic unit improve the energetic contribution of polysaccharides to EPS structural stabilization. Higher humic substance and carboxyl groups content primarily weaken the structural strength of ADS EPS. In general, this study proposes a powerful approach for investigating the molecular choreography within EPS, utilizing atomic simulations based on solved structures to explore the contribution of specific biopolymer features to structural energetics, providing theoretical insights to guide EPS-engineered regulation in wastewater treatment processes.

Keywords: extracellular polymeric substances, molecular dynamics simulations, EPS cluster model, activated sludge process, biopolymer identification and modeling

Competing Interest: The authors declare no competing interests.
Received: August 14, 2024. **Accepted:** April 22, 2025

Significance Statement

Structural properties of extracellular polymeric substances (EPSs) determine the immediate environment for microbial survival and characterize biofilms. Aerobic activated sludge and anaerobic digestion sludge processes are essential for global wastewater purification and organic matter resource conversion and recovery; unraveling their EPS compositions and functionalities can better guide process innovations. Limitations of current characterization methods cause gaps in the fundamental knowledge of EPS generation and functions. Here, we provide a brute-force molecular dynamics approach for resolving EPS clusters and construct several representative EPS cluster models through molecular characterization and modeling. The results of the modeling analysis provide valuable insights into the formation pathways and biopolymer arrangement rules of EPS clusters.

Introduction

Activated sludge process is the most prevalent biological wastewater treatment technology and will continue to play an irreplaceable role in wastewater treatment plants (1, 2). Activated sludge consists of microorganisms in forms of flocs, granules, or biofilms (3). Flocs including aerobic activated sludge (AAS) and anaerobic digestion sludge (ADS) are commonly used in wastewater purification and organic resource conversion, whose performance has a considerable impact on the overall efficiency and environmental effects of wastewater treatment plants (4, 5). Extracellular polymeric substances (EPSs) from microorganisms represent the main components of the agglomerate matrix, and their composition, properties, and dynamics have substantial effects on the microbial activities and sludge characteristics (6–8). Transformation of hydrophilic components and functional groups in AAS EPS causes changes in sludge properties during anaerobic digestion (9, 10). EPSs contribute to various biopolymer structural properties (adsorption, hydrophilic/hydrophobicity, and viscoelasticity) due to their complex origin and formation process (11). The resulting structures protect microbial cells against the external environment and allow microbial aggregates to perform biochemical functions at the cell interface (12, 13). Additionally, the effect of EPS surface properties on sludge floc determines the effluent quality and resource recovery efficiency of the treatment system (14, 15). Thus, investigation of EPS structural properties enables engineering and process optimization of current wastewater treatment and biosolid management. AAS and ADS contribute significantly to global wastewater purification and resource recovery, but their EPS structural properties are still far from fully resolved.

From the expanded analytical and biomolecular engineering techniques, several structural information and functions of EPS in activated sludge have been identified (16, 17). Isolation and enrichment followed by molecular characterization are used to study biopolymers in EPS, through which the molecular structures of several representative proteins and polysaccharides (PSs) have been proposed via mass spectrometry and spectroscopy (18–20). However, some argued that this in vitro characterization technique only obtains a portion of the EPS landscape, and the results are susceptible to the extraction method. In addition, the status of key biopolymer components in EPS remains unclear, leaving their function poorly defined. In situ characterization techniques can offer a nondestructive identification of EPS molecular structure and probing of the distribution dynamics of specific biopolymers (2, 21). Several in situ microimaging and spectroscopy techniques have been applied to reveal the compositional properties of EPS and their effects on the physicochemical properties of activated sludge (16, 22, 23). Nevertheless, it is still a great challenge to directly obtain the structure of gel-like networks in detail using the current in situ approaches due to the complex and heterogeneity of EPS (24). Methodological limitations lead to a largely unexplored in the generation and modulation of EPS molecular clusters (25).

Molecular dynamics (MD) simulation is an effective tool for tracing atomic-scale phenomena in environmental sciences, which is ideal for quantitative predictions of compound interactions in EPS (26, 27). MD simulations have been extensively employed to explore the self-assembly process and interaction dynamics of biochemical compounds in previous studies (28–30). Recent studies have increasingly used MD simulations to calculate the EPS 3D structure and assess the effect of biopolymer composition on cluster properties (31, 32). Similarly, a simplified EPS model was constructed in our previous work to elucidate the effect of multivalent cations on EPS properties (33). These simulations were based on a limited number of presumed macromolecules in the absence of realistic molecular structural details, despite the fact that EPS is a heterogeneous mixture of numerous molecules (34, 35). Models with more versatile and realistic components are needed for the accurate reflection of EPS structure and aggregation behavior.

In this work, the representative structures of biopolymer components in two typical floc sludge (AAS and ADS) EPSs were presented through characterization and screening. Then, the biopolymer molecular models constructed based on structural analysis were used in large-scale MD simulations to establish realistic EPS models for the first time. Spatial redistribution processes directed by noncovalent interactions among components were traced by simulations during the formation of individual EPS molecular clusters. Moreover, the findings of model analyses promoted the understanding of the modulation mechanisms of key molecular features in each component on the formation pathways and structural properties of EPS (Fig. S1).

Results and discussion

Characterization of EPS composition and key component structures

The composition of six basic biopolymers in AAS EPS and ADS EPS was analyzed to screen for potential candidates to be included in the EPS model (Fig. 1a). Proteins are predominant in both EPS samples, followed by PSs) and humic substances (HSs). The HS content of sludge EPS increased significantly after anaerobic digestion, whereas the content of protein and PS decreased. Proteins, PSs, and HSs represented more than 80% of the EPS composition, so detailed structural screening of these key biopolymer components was implemented. To quantify highly abundant extracellular proteins in AAS and ADS, iBAQ algorithm was used. The detected proteins in AAS EPS and ADS EPS ranked by the iBAQ value are presented in Fig. 1b and c and Tables S1 and S2. The results of high-performance size exclusion chromatograph (HPLC-SEC) (Table S3) and sodium dodecyl sulfate–polyacrylamide gel electrophoresis (Fig. S3) showed the molecular weight (MW) of the

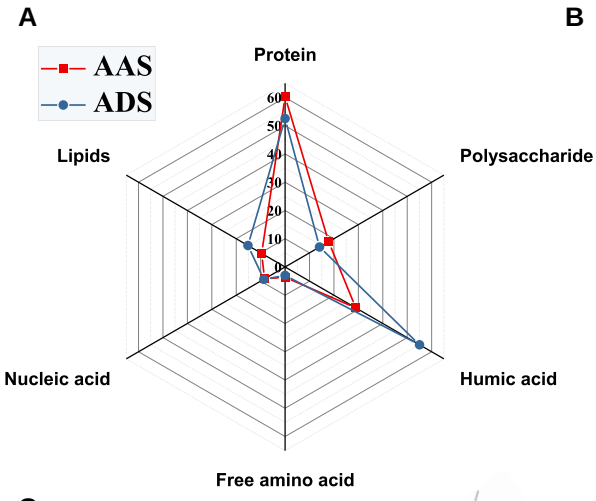

B

AAS EPS Protein IDs	iBAQ (×10⁷)	Intensity (×10⁸)	MW (kDa)	Secondary Structure H	E	L
A0A940L8G8	**11.3**	3.39	**18.636**	13.15	18.78	68.08
A0A4Q7N0U8	6.34	15.2	49.943	60.77	10.2	29.02
A0A5B8UNY1	4.47	1.34	18.212	5.75	27.59	66.67
I0AI43	3.51	**4.98**	**24.353**	36.06	15.38	48.56
A0A9D9MY39	2.85	3.42	24.058	28.19	12.78	59.03
A0A940LA56	1.65	5.84	43.141	25.82	34.43	39.75
A0A9D9QRV0	1.50	0.90	10.472	64.36	0	35.64
A0A1A9HZF8	1.47	2.94	36.783	51.1	15.67	33.23
A0A495WCH1	1.32	0.81	**13.886**	15.45	**47.15**	37.4
A0A9D9W5D2	1.27	0.76	13.506	30.83	13.33	55.83

ADS EPS Protein IDs	iBAQ (×10⁷)	Intensity (×10⁸)	MW (kDa)	Secondary Structure H	E	L
A0A660HSC1	**27.1**	43.3	**28.019**	34.68	11.69	53.63
A0A660HSY9	17.0	29.6	73.464	6.49	52.79	40.72
A0A660HSG9	15.7	24.1	45.524	48.39	16.82	34.79
A0A660HRY1	8.51	24.6	62.22	53.24	9.11	37.65
A0A660HT81	7.32	3.87	20.812	8.47	49.21	42.33
A0A1M4UPB4	6.35	1.90	**14.084**	46.56	19.85	33.59
A0A660HQ47	5.79	17.6	52.636	29.45	23.73	46.82
A0A660HR24	5.24	4.39	**14.764**	17.29	**39.1**	43.61
A0A3F3S6D4	4.39	2.33	10.07	41.3	18.48	40.22
A0A660HQH1	3.47	2.77	12.331	95.41	0	4.59

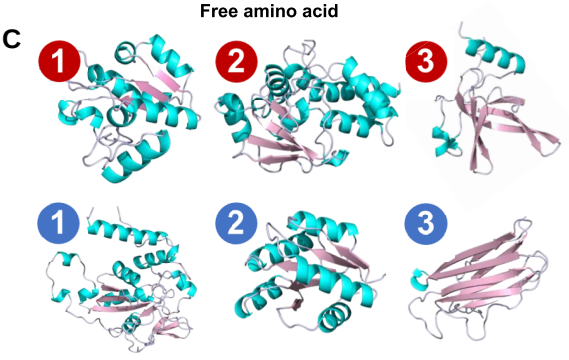

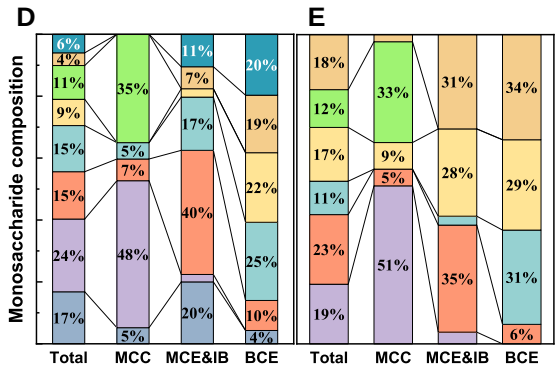

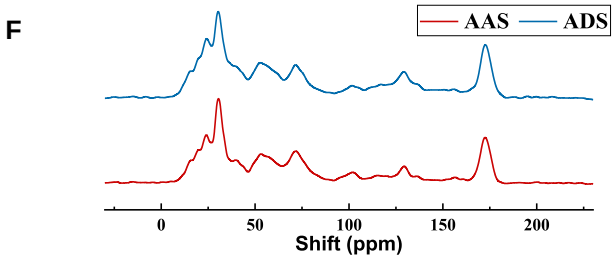

Shift (ppm)	0-50	50-90	90-110	110-162	162-185
Description	Aliphatic-C	Carbohydrate-C	Acetal-C	Aromatic-C	Carboxylic-C
Fraction(AAS)	**0.4**	**0.284**	0.048	0.148	0.12
Fraction(ADS)	0.32	0.222	0.053	**0.236**	**0.17**

Fig. 1. Sludge EPS composition and molecular features. a) Biopolymer concentration in AAS and ADS EPS (normalized by sludge total suspended solids [TSS], concentration in mg/g TSS); b) abundant proteins in AAS and ADS EPS ranked by the iBAQ scores; the accession ID is UniProt ID; intensity is the raw intensity value of the mass spectrometry signal of the identified PEs; protein secondary structure composition (%) obtained from PredictProtein; the proteins selected as model constructs in AAS and ADS are highlighted in the table, respectively; c) structures of proteins selected for EPS model construction; AAS and ADS proteins are labeled with serial numbers, respectively; monosaccharide composition of each part in AAS (d) and ADS (e) extracellular polysaccharide (main chain core [MCC], main chain edge [MCE], inner part of the branch [IB], branch chain edge [BCE]); f) 13C NMR spectra and chemical shifts of HSs in AAS and ADS EPS.

sludge extracellular protein was mainly distributed in the range of 10–30 kDa. Thus, A0A940L8G8 and I0AI43 were selected as representative extracellular proteins for AAS EPS models, whereas A0A660HSC1 and A0A1M4UPB4 were selected for ADS EPS model construction. In addition, A0A495WCH1 and A0A660HR24 were supplementarily chosen as high β-sheet structural protein representatives for the EPS model, since proteins with a high amount of β-sheet structure exhibited extensive building potential in the biofilm matrix (36).

The monosaccharide composition of each part in the AAS and ADS EPS is shown in Fig. 1d and e. AAS EPS was more complex and contained acidic sugar units. Methylation analyses (Tables S4 and S5) showed that AAS and ADS EPSs had the same terminal sugar residues (T-Araf, T-Glcp, T-Galp). However, the branching points of AAS EPS occurred at 1,3,4-Rhap and 1,2,3-Fucp, and those of ADS EPS mainly occurred at 1,3,4-Rhap. The analysis of MW showed that AAS and ADS EPSs had distributions around 1.5 and 3 kDa, respectively, indicating that PSs have two chain lengths with similar repeating units in both AAS and ADS EPSs. Therefore, based on the sugar residue content and glycosidic linkages, potential structures of AAS and ADS EPS were proposed as shown in Fig. S4. Particularly, galacturonic acid was detected at terminals in both the main chain and branched chains of the AAS EPS, so two PS models were constructed accordingly. As

shown in Fig. 1f, the percentage of aliphatic and carbohydrate structures in extracellular HS decreased after anaerobic digestion, whereas the aromatic degree and carboxyl groups content increased. Based on analytical results of functional groups, organic element content (Table S6), and MW, HS molecules were constructed using VSOMM2 and optimized according to the percentage of carbon types.

Subsequently, different biopolymers were selected and incorporated into the models to represent EPS in AAS and ADS, including proteins, peptides (PEs), PS, HS, lipid (LIP), amino acid, and nucleic acid (NA) (Table S7). Initial individual EPS clusters were constructed using these biopolymer model units, where each cluster has a protein as its main chain with the remaining units added based on the designated compositions. Multivalent cations including Ca^{2+}, Mg^{2+}, Al^{3+}, and Fe^{3+} were added with concentrations matching the average analytical results (Table S8). The remaining negative charges were neutralized using Na^{+}. Thus, three models were constructed for each sludge EPS as representative individual cluster models using different protein main chains, with the biopolymer unit composition given in Tables S9 and S10. In addition, three extra parallel simulations of AAS1 and ADS1 clusters were performed, and the initial positions of components in each parallel cluster were rearranged to evaluate the reproducibility of the simulated results; the initial system snapshots of the raw and parallel simulation clusters are shown in Fig. S5.

Molecular arrangement and interaction properties of biopolymers in EPS

The stable clusters of EPS with a supramolecular structure were obtained by MD simulation, and the radii of gyration (R_g) of the clusters are shown in Fig. S6. All clusters converged and stabilized after 100 ns alone with a plateau in R_g. Therefore, the last 50 ns of trajectories was used to analyze the dynamic structural properties of clusters. As shown in Fig. 2a and b, the probability distribution function (PDF) for the distribution of biopolymers from the cluster center of mass (COM) shows that protein main chain (PRO) resides mostly in the cluster core due to its high content percentage surrounded by the remaining components. AAS EPS clusters had a denser structure than ADS EPS clusters, which may be related to the charge carried by the biopolymer molecules, especially the PRO. AAS2 clusters presented a more compact biopolymer arrangement, whereas AAS3 and ADS3 clusters containing PRO composed mainly of *β-sheet* had a looser structure. In addition, the distance of HS molecules COM to the cluster COM in ADS EPS decreased with the increased ratio of HS content, suggesting the influence of HS components on cluster properties increased. Spatial distribution function (SDF) (Fig. 2c and d) showed the 3D density distribution of components in dynamic clusters. The biopolymer molecules evenly formed a layered structure around the PRO, and small molecule acid (SMA) molecules were mainly on the periphery with a wide motion range. Other molecules with similar structure properties and function did not show an obvious pattern of rearrangement. Their distribution in the cluster depends on the initial position and molecular interactions.

The average minimum distances between the components, i.e. contact maps (Fig. 2e and f), quantify the molecular interaction in clusters. The color mapping of the minimum distance is set to make a distinct color at interresidue distances <0.45 nm. Short-range contacts below 0.45 nm are the mainly cohesive source of clusters, including salt bridges, hydrogen bond, and hydrophobic interactions between residues. PRO played an essential role in aggregating the remaining molecules and stabilizing the clusters in all models. PE and PS molecules formed many short-range contacts with HS, PRO, and other biopolymers concurrently. The PDF and SDF results indicated that PE and PS play a pivotal role in tandem molecules in clusters. Meanwhile, the increase in the number of HS chains in ADS clusters did not lead to a significant increase in contact with other components, indicating that concentration is not the primary factor influencing the effective interactions among biopolymers and other components. As shown in Fig. 2e and f, few salt bridges were formed among biopolymer molecules since many molecules contained only negatively charged groups. Amino groups in the protein fractions (PRO, PE, and free amine acid [FAA]) are positively charged, so salt bridges were mostly formed between proteins and HS molecules (Fig. S7). Besides salt bridges and a large number of hydrogen bonds, other short-range contacts of residues include hydrophobic interactions and molecular entanglements also played important roles in maintaining the configuration of biopolymers.

Aggregation pathway and structural properties of EPS cluster

Residue contacts generated functional group bridging, leading to a decrease in solvent-accessible surface area (SASA) during the biopolymer aggregation processes. As shown in Fig. S8, a noticeable decrease occurred in both hydrophilic and hydrophobic SASA of biopolymers during the cluster formation process, suggesting that EPS cohesion is a cooperation of polar and nonpolar interactions. Stabilized EPS cluster surfaces were abundant in both hydrophilic and hydrophobic regions (Fig. 3a). The hydrophilic surface was mainly provided by oxygen- and nitrogen-containing groups, while the hydrophobic region was basically composed of carbon- and hydrogen-containing groups (Fig. S9). Compared with AAS, the exposed area of nitrogen-containing polar groups in ADS cluster was reduced, suggesting a decrease in the contribution of protein-like fractions to the surface properties of EPS.

Free energy surfaces (FESs) of AAS1 and ADS1 were calculated along two process variables, the ratio of hydrophobic and hydrophilic SASA, representing the occupancy degree of nonpolar and polar active regions, and the R_g of clusters, representing the degree of biopolymer aggregation. The FES landscapes for different time frames (0–200 and 70–200 ns) are shown in Figs. 3b and S10. An approximate diagonal pathway can be observed from the initial state to the biopolymer fully associated state in both clusters, especially in ADS1. Thus, polar functional groups were more utilized for biopolymer chain association during cluster formation. Similar results were observed from SASA change in biopolymer components, where the hydrophilic surface area percentage of all molecules except LIP decreased after cluster formation (Fig. S11). In addition to a deep energy well representing the final state, several shallow wells, representing the transition substates, were presented in the FES of AAS1 and ADS1, suggesting the formation of EPS clusters occurred on a rugged energy landscape with multiple minima on the path to the final ordered state, a scenario reminiscent of protein and RNA folding (37, 38). ADS1 has more transition substituents than AAS1 during cluster stabilization; in other words, biopolymer aggregation in ADS undergoes a more rugged process. Consistent sources of biopolymer noncovalent interactions led to the similar dynamic modulation process of AAS and ADS clusters. The free energy extended to areas with higher hydrophobic SASA ratio and lower R_g, while the hydrophobic SASA proportion decreased with the formation of the final stable clusters, indicating the contribution of the hydrophobic groups in the cluster further stabilization.

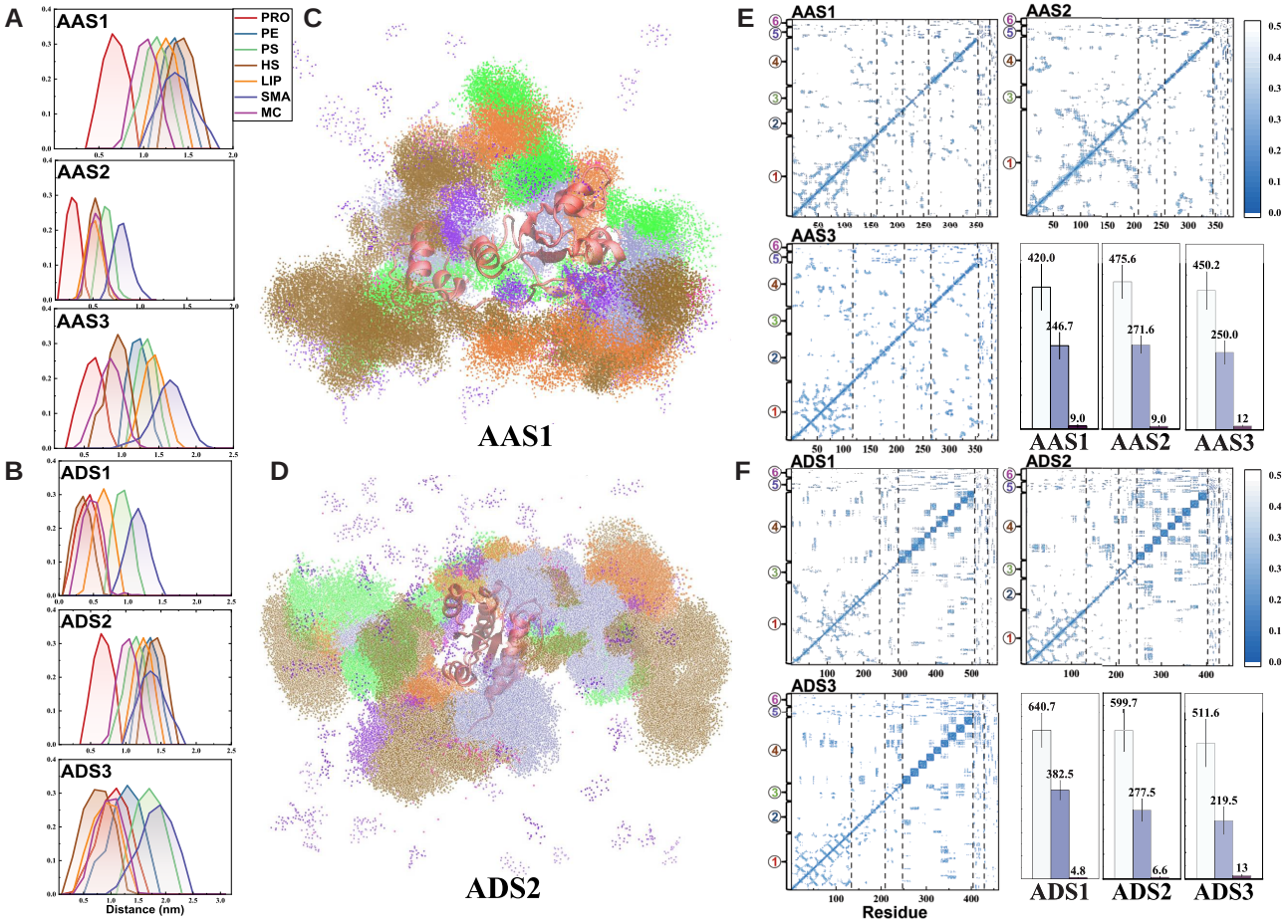

Fig. 2. Molecular arrangement and interaction dynamics of components. a) PDF for the distribution of the component molecules in AAS EPS; b) PDF for the distribution of the component molecules in ADS EPS; SDF of components (PE, PS, HS, LIP, SMA, and multivalent cation [MC]) around PRO in AAS1 (c) and ADS2 (d); color codes for the component are the same as in the PDF: PRO: red, PE: blue, PS: green, HS: brown, LIP: orange, SMA: violet, and MC: magenta; average minimum distance (contacts) between various components (1: PRO, 2: PE, 3: PS, 4: HS, 5: LIP and SMA, and 6: MC) and number of (from left to right) residue contacts (with a cutoff distance by 0.45 nm), hydrogen bonds, and salt bridges in AAS (e) and ADS (f) EPS cluster.

MD snapshots of biopolymers in three states of ADS1 were extracted for solidification and observation of functional group interactions during cluster stabilization (Fig. 3c). The representative structure at state 1 (HPO SASA/HPI SASA, R_g) = (0.87, 3.38) showed that the biopolymer formed a major agglomerate and several small agglomerates, a common state of EPS clusters, with free energy barriers formed by the negative surface charge keeping the agglomerates dispersed (31). In contrast to AAS, more negatively charged biopolymers in ADS EPS make it easier to form multiple temporary clusters balanced by negative potential barriers, leading to more intermediate states in the formation of ADS1 clusters. When the contact between polar groups generated effective interactions to break the barrier, the agglomerates were further assembled to reach a metastable state 2 (0.89, 3.3). Subsequently, agglomeration-promoted molecular interactions (hydrophobic interactions and hydrogen bonding) triggered structural transition to a more stable state 3 (0.88, 3.24). This process elucidates a potential mechanism of initial EPS matrix formation, where individual molecular chains or small clusters are incorporated into the matrix by ionic interactions and subsequently stabilized by hydrogen bonds and hydrophobic interactions. Molecular arrangement depends on where effective contact occurs, and the random distribution of biopolymers in wastewater treatment systems contributes to the heterogeneity and complexity of the resulting EPS matrix. This is also reflected in the parallel simulations of AAS1 and ADS1, where differences in initial positions lead to variations in the generation of component interactions, resulting in distinct aggregation processes among parallel clusters (Fig. S12). However, all parallel systems form a layered assembled cluster centered around PRO after 100 ns of simulation. Meanwhile, AAS1 parallel clusters have a more compact structure than ADS1 parallel clusters. The partial distribution of components and groups differs greatly among parallel clusters (Fig. S13), whereas the cluster size and surface properties remain similar (Fig. S14). Therefore, the composition and structure of the components determined EPS macroscopic properties.

As shown in Fig. 3d, the average binding energy of biopolymer molecules was calculated (method given in Text S7) for each model of AAS and ADS. The average electrostatic repulsion between biopolymers in ADS clusters is higher than that of AAS, suggesting a larger energy barrier to overturn in ADS clusters. Van der Waals (VDW) forces from hydrophobic interactions in each cluster were similar and favorable for stabilization. In addition, the results of binding free energy showed that all clusters except AAS2 are hard to spontaneously aggregate and reach the final steady state in the absence of metal ions. Tighter intermolecular interactions gave AAS clusters a more stable structure than ADS.

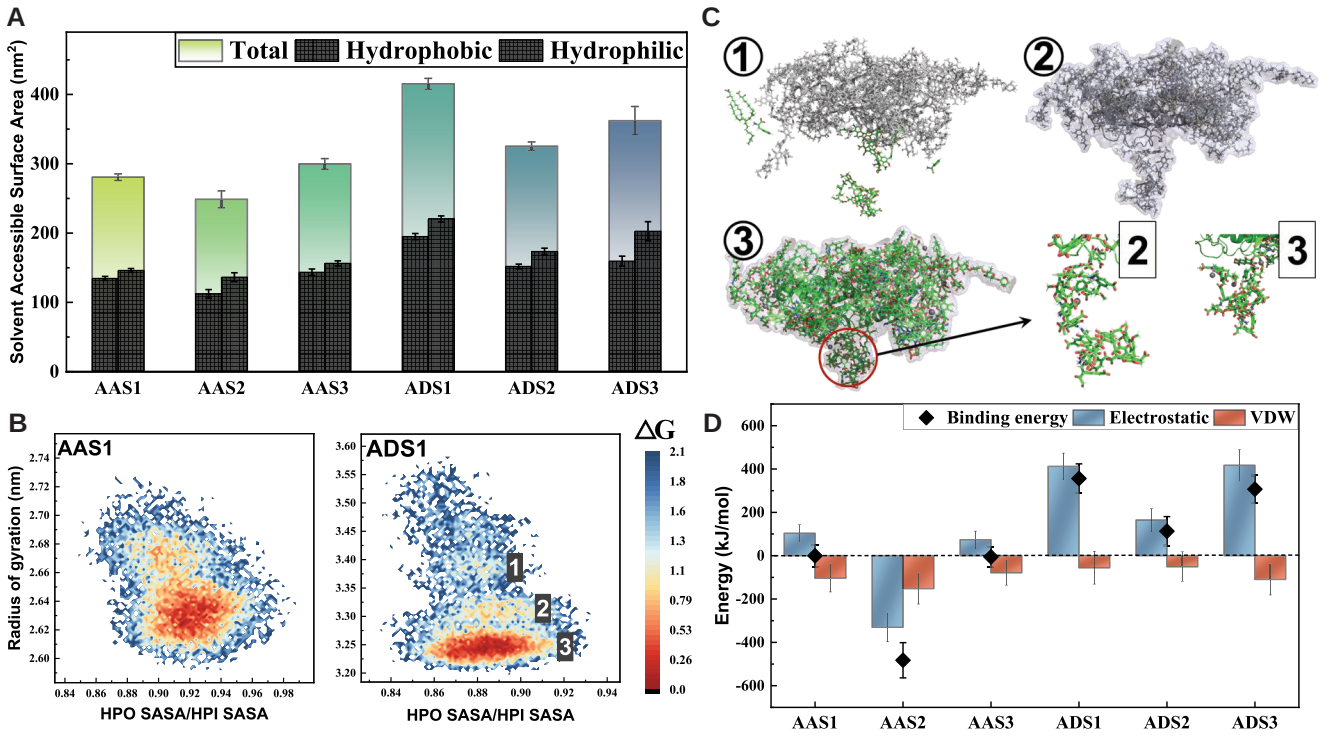

Fig. 3. Assembly energetic dynamics and structural properties of EPS clusters. a) The SASA of the stable clusters in each system; b) free energy landscape spanned on hydrophobic (HPO) SASA/hydrophilic (HPI) SASA and radius of gyration for 70–200-ns process in AAS1 and ADS1 model; c) representative MD snapshots of cluster structures in three states of ADS1 (corresponds to number in b) and details of functional group interactions in the transition from state 2 to state 3 (lower right); major aggregate and small aggregates were distinguished by color in state 1 and state 2; d) average binding free energy of biopolymer molecules to maintain cluster stability in each system.

Large clusters of AAS and ADS EPS were constructed using the individual cluster models, respectively, to investigate the aggregation behavior of the cluster during the broader EPS matrix formation process (Fig. S15). The contact numbers among individual clusters were used to trace the formation and stabilization of molecular clusters (Fig. S16a), interaction of biopolymers in AAS and ADS clusters stabilized after 150 ns. The formation of larger clusters followed by the decrease in hydrophobic and hydrophilic SASA (Fig. S16b), suggests the formation and stabilization of large clusters also rely on the interactions between polar and nonpolar groups. The spontaneous formation of large clusters had no obvious and regular effect on the surface properties of individual clusters (Fig. S17a–c). Surface properties determined by the biopolymer molecular features and arrangement were the basis for interactions among individual clusters and capture of other molecules. Thus, the stabilization process of large clusters was similar to the individual cluster aggregation behavior, and AAS clusters showed a more stable structure (Fig. S17d and e).

Modulation mechanism of components on EPS formation and structural properties

To further clarify the role of biopolymers in the formation and stabilization of EPS, the effect of different features in each individual component on structural formation of EPS was then investigated. The contributions from each component to the total SASA can be further parsed into information on the surface-active property (Fig. 4a). PRO, PS, and SMA fractions had similar hydrophobic and hydrophilic SASA in each system, whereas PE and LIP contributed more to hydrophobic surface area. Of particular interest is that HS not only represented the majority of hydrophobic SASA in EPS, but also contributes the most hydrophilic SASA. As shown in Fig. 4b, PRO was favorable for component aggregation and stabilization in each cluster as predicted above, and positively charged AAS PROs had the stronger binding capacity. PS also contributed to the maintenance of cluster stability in each system, whereas the presence of HS was almost detrimental to biopolymer aggregation.

Protein

As shown in Figs. 4c and S18, the binding energy between PRO and the remaining components in each system was grouped based on the residues corresponding to the secondary structure (*α-helix* with green background, *β-sheet* with pink background). The binding energy among *α-helix* residues and other biopolymers was higher than the residues comprising *β-sheet* structure in all systems. Even in ADS3 cluster, PRO consists almost entirely of *β-sheet* structure; the average binding energy between the *α-helix* residues and other components is still significantly higher than *β-sheet* residues. Meanwhile, the contact numbers between PRO residues and the remaining biopolymers in each system were counted (Fig. S19). The contacts with *α-helix* residues showed no significant difference from *β-sheet* residues in each PRO ($P > 0.05$), indicating that the residues were not enhancing the aggregation capacity of *α-helix* structure by generating more interaction points. As representatives of the abundance *α-helix* and *β-sheet* structures, the corresponding structural residues in AAS2 and ADS3 were picked for further analysis (Fig. 4d). The results of MD snapshots and binding energy compositions indicated that the *α-helix* structure contained more polar groups than *β-sheet*, forming numerous polar effective interactions including hydrogen bonds and salt bridges. These polar interactions provided higher binding energies than the hydrophobic interactions

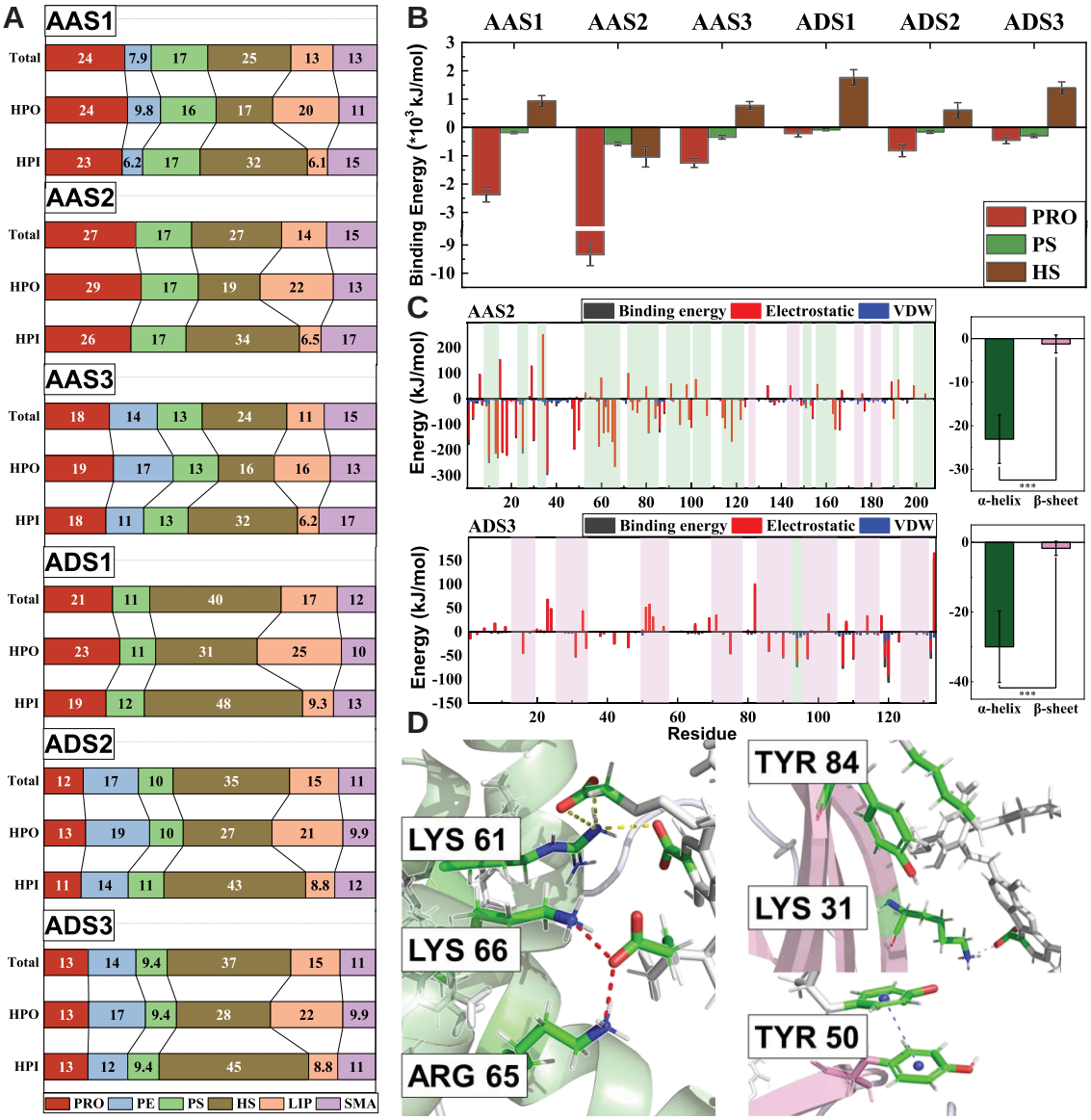

Fig. 4. Contribution of key components to EPS structural properties. a) Component contribution to cluster SASA; b) average binding free energy of PRO, PSs, and HS contributions to cluster stabilization; c) contribution of the PRO residue to the binding free energy with remaining molecules (residues corresponding to the α-helix and β-sheet structures are labeled with green and pink backgrounds, respectively) and average bind free energy with remaining molecules of α-helix and β-sheet structures; d) representative MD snapshots of protein residues in AAS2 and ADS3 interacting with the remaining molecules (labels are amino acid names and serial number of residue corresponding to c); protein secondary structure shown as cartoon; specific residues shown in stick form; color codes for atoms: green: C, red: O, blue: N, white: H, interactions marked with dotted lines: red: salt bridge, yellow: hydrogen bond, and blue: hydrophilic interaction.

in the *β-sheet* structure, enhancing the aggregation efficacy of the *α-helix* structure for biopolymer molecules, thus resulting in a denser molecular network in the system with PRO composed mainly of *α-helix*. PROs with larger MWs and more residues could support more contacts and interactions with other molecules (Fig. 2e and f), but the binding free energy of PRO in ADS1 was not higher than other ADS. AAS PROs (especially AAS2) with more positively charged groups possessed a higher binding free energy. Therefore, the composition and distribution of polar groups are key determinants of protein modulation capacity.

Polysaccharide

PS components in AAS and ADS clusters have similar contributions of surface amphiphilicity and binding free energy. In contrary to the results of previous EPS model, PS was favorable for component aggregation in each cluster (33). Monosaccharide composition caused this discrepancy. The abundance sugar unit in AAS and ADS consists of fructose, rhamnose, and arabinose, where hydroxyl and hydrocarbon groups provide the basis for hydrogen bonding and hydrophobic interactions between the PS and the remaining components. Thus, there are both sizable polar and nopolar components in the binding free energy of most residues (Figs. 5a and S20a). Remarkably, residues with high affinity were mainly found at the periphery of the PS chain. The average binding energy and the contact number between the residues and the remaining molecules progressively increased with the distribution position shifting outward in all systems (Figs. 5b and S20b), which suggested that the residues on branched chains

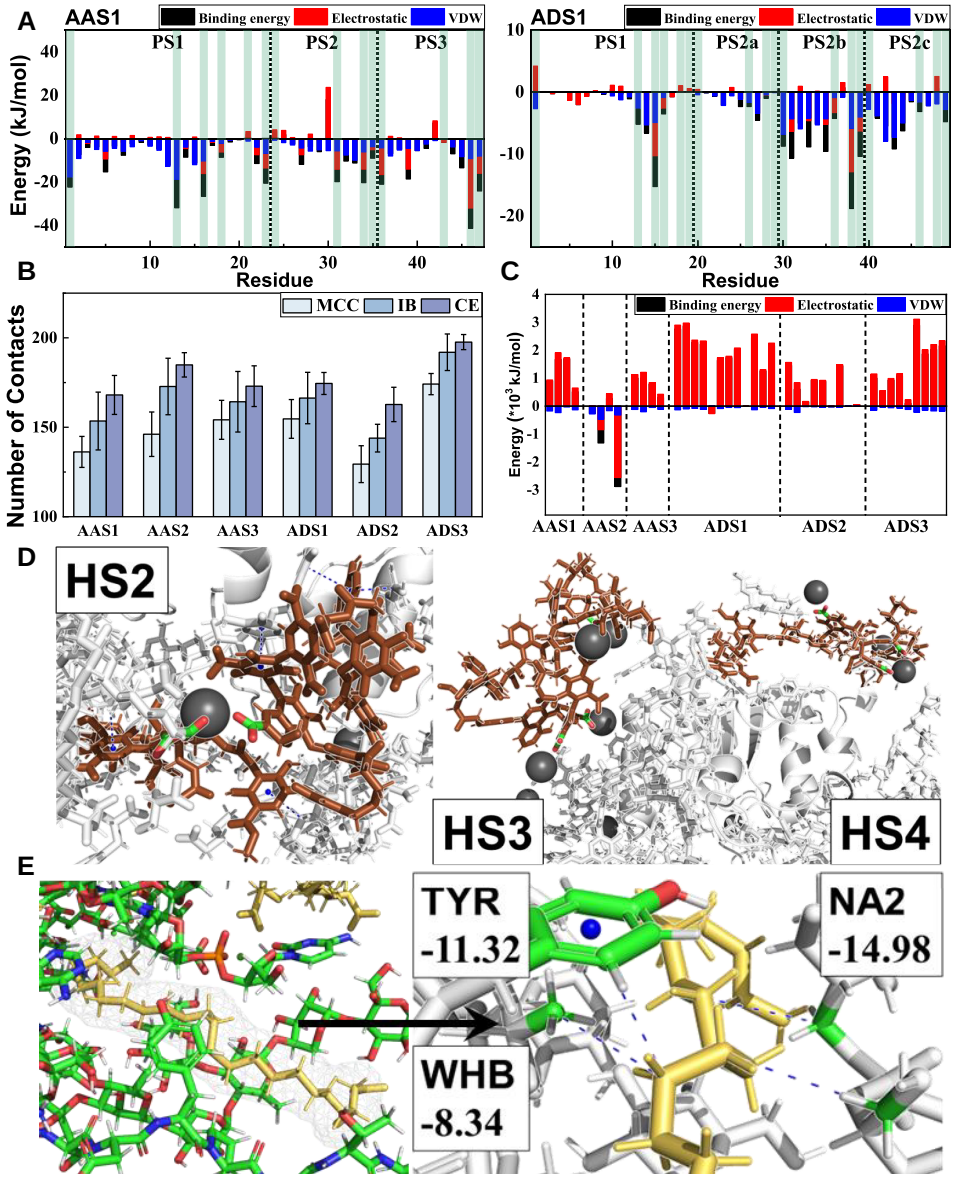

Fig. 5. Modulation mechanism of component structural features on EPS cluster properties. a) Contribution of the PS residue to the binding free energy with remaining molecules; b) contact numbers between residues in each part of the PS chain and remaining molecules. MCC, main chain core; IB, inner part of the branch; CE, chain edge (including main chain edge and branch chain edge); c) binding free energy between HS chains and the remaining molecules in each cluster; d) representative MD snapshots of the interaction between HS chain and the remaining molecules in AAS1; e) representative MD snapshots of LIP as a hydrophobic bridge in clusters; hydrophobic interactions were marked with blue dotted lines, labeled as the residue or molecule creating the interaction and binding free energy (kJ/mol).

and the edge of the main chain have high interaction efficiency. Similarly, galacturonic acid unit on the PS branched in AAS possessed a higher contact efficiency with cationic groups compared with the units on the main chain (Fig. S21). Meanwhile, the diverse glycosidic linkage and branching structure result in the stretching of the PS molecular chains in the EPS clusters, enhancing the contact efficiency between the residues and the remaining molecules (Fig. S22). These factors promoted the modulation of cluster stability by PS.

Humic substances

HS dictated the surface properties of EPS. Although HS generally considered representative of hydrophobic functional group possessors, the result of SASA suggested that HS contributed more to the hydrophilic region of the EPS cluster surface. Especially in ADS EPS, HS occupied nearly half of the hydrophilic surface area of the cluster. The abundance of oxygen-containing functional groups elevated the contribution of HS molecules to the polarity of EPS, among which carboxyl groups imparted electrostatic repulsion between HS and the remaining components that interfered with the self-assembly and stabilization of clusters. The average binding energy of these interactions consisted of mostly electrostatic repulsion and slight VDW (Fig. 5c). The higher HS content in ADS brought more instability to the clusters than AAS. The decrease in MW, carbohydrate-C, and aliphatic-C content resulted in the chain shortening in HS after anaerobic digestion, resulting in a more effective charge density enhancement from increased carboxyl group content (Fig. S23). Thus, the molecular electrostatic repulsion was further enhanced, and the

stability and compactness of EPS cluster were reduced. It is noteworthy that the increase in the aromatization degree of ADS HS brought no significantly increase to the VDW component of the binding energy, which is attributed to the electrostatic repulsion induced by carboxylate groups that prevented the short-range intermolecular contacts and affected the hydrophobic interactions between the aromatic groups. Although the results of the radial distribution functions (Fig. S24) proved the presence of hydrophobic interactions in the main contacts between HS and the remaining molecules, the interactions between polar groups determined the function and distribution of HS in EPS clusters, which was also corroborated by the changes in SASA (Fig. S11). Representative MD snapshots (Fig. 5d) showed the behavior of three molecular chains with different VDW components in AAS1. Cation-assisted contact of HS2 with molecules inside clusters promoted hydrophobic group interactions, whereas the distribution of HS3 and HS4 on the cluster surfaces caused the lack of opportunities for effective hydrophobic interaction. Electrostatic repulsion affected the short-range contact between HS and other molecules, preventing effective hydrophobicity interaction and placing the HS chains at the cluster surface.

Other components

The contributions of LIP, SMA, and metal ions to cluster formation in the EPS model were also investigated. LIP was the only component interacting with other molecules mainly through hydrophobic groups, because of its chain structure. Although LIPs might suffer from electrostatic repulsion between the head carboxyl group and the remaining molecules, the hydrocarbon structure provided active hydrophobic interaction sites (Fig. S25). Thus, the LIP molecules distributed in the cluster interior acted as hydrophobic bridges of the remaining molecules (Fig. 5e). LIP molecules distributed at the cluster periphery interacted with aromatic groups in HS, resulting in hydrophobic pockets on EPS (Fig. S26). Affinity between the SMA component and the remaining components was observed in all systems (Fig. S27a). SMAs were hardly immobilized in the cluster since short molecular chains were unable to generate multiple effective contacts simultaneously. Therefore, SMA component showed an external and wide distribution in clusters, presented higher capacity of free diffusion than other components in each system (Fig. S27b). High mobilization properties impart roles to SMA components in intercluster and intercellular communication and source transfer.

Metal ions, especially multivalent cations, were imperative in the formation and stabilization of clusters. Most of the clusters, especially ADS clusters, will not be formed and stabilized successfully in the absence of metal ions. Multivalent cations promoted cross-linking between biopolymers via electrostatic salt bridge networks (Fig. S28). ADS has more abundant negatively charged groups, requiring more multivalent cations to promote biopolymer aggregation and maintain its structure than AAS. Complexation sites in ADS can further trap cations and enhance the bioavailability of metal ions. Electrical neutralization and bridging provided by metal ions reduce electrostatic repulsion between biopolymers and facilitate intermolecular contact. Based on these mechanisms, the injection of multivalent cations during water treatment can significantly alter the EPS clusters. The bridging of negatively charged functional groups by multivalent cations can cause the rearrangement of biopolymer components, modify the polar functional groups distribution on cluster surfaces, and reduce the hydrophilicity surfaces. Meanwhile, more metal cations will further promote the short-range contact between biopolymers, improve the hydrogen bonding and hydrophobic interactions between biopolymer molecules, and enhance the density and stability of EPS clusters (33). Trivalent cations of Fe^{3+} and Al^{3+} had higher bridging efficacy due to the charge number, but in relatively low quantities (Fig. S29a and b). The major bridge provider in clusters was the most abundant Ca^{2+} (Fig. S29c). In addition to bridging, the neutralization of negatively charged groups by cations had a significant role in promoting biopolymer aggregation. The binding energy between the HS and cluster neutralized by Na^{+} was significantly higher than in the absence of Na^{+} (Fig. S29d).

The results of interaction analysis and energy calculations elucidated the functional contributions of each component to EPS clusters, and the molecular arrangement and interaction properties of each component and their modulation mechanisms on EPS structural properties of EPS are given in Table 1. However, despite the detailed investigation of typical components in EPS, certain biopolymers possessing different structural features (e.g. amyloid and cellulose) remain underexplored. Further characterizations and simulations are needed to reveal the specific roles of these components in EPS formation and functionality.

Potential implications

EPS structure properties are known to determine the morphology and physicochemical characteristics of activated sludge in wastewater treatment system (33, 39). The diverse composition and flexible arrangement of biopolymers provide microbial aggregates with a highly adaptable infrastructure, as well as contributing to the EPS complexity and heterogeneity, resulting in impediments to the investigation of EPS aggregation dynamics and structural properties (24, 25). In this study, we built realistic EPS cluster models by combining chemical characterization and MD simulations and tracked the component functional interactions at atomic scale. The role of polar interactions (salt bridges, hydrogen bonds) and hydrophobic interactions in the EPS formation and stabilization process were clarified, and key molecular factors modulating such complex dynamic processes in different biopolymers were revealed. Simulation results provided the microscopic molecular validation and presentation of important inferences for previous EPS studies, which shed light on the molecular functions of key components to a nearly in situ level (40, 41). These insights provided guidance for EPS production and conditioning engineering. For instance, injection of positively charged groups or controlling pH can reduce the rugged process in biopolymer aggregation and EPS formation. Identification of the components that dominate the structural properties of EPS can provide a basis for targeted regulation of AAS and ADS. More attention can be focused on the regulation of the protein component during AAS EPS treatment process, e.g. to reduce the hydrophilicity of the EPS by modulating the conformation of protein through the polar solution. In contrast, the regulation of ADS EPS can focus on the HS components, such as using multivalent metal ions or cationic polymers to enhance the cohesion between HS and biopolymer molecules. Meanwhile, the retention of hydrophobic toxicants by HS and LIP during sludge anaerobic digestion process should be further considered. Additionally, the impact of key component variations in influent from different regions on EPS structural properties also warrants attention. For instance, an increase in organic matter content in influent can lead to larger EPS cluster sizes, while a rise in heavy metal ion concentrations can promote EPS aggregation, resulting in more compact sludge flocs (42). Molecular characterization and biopolymer screening allowed

Table 1. Summary of analytical results for each component in EPS cluster.

Components	Molecular arrangement and interaction properties	Modulation mechanism on EPS structural properties
Protein main chain	Located at the cluster core, interact most frequently with the remaining components	Critical for aggregating the remaining molecules and stabilizing the clusters, polar groups in the *α-helix* enhanced aggregation efficiency
Polysaccharide	Distributed between central and peripheral components, forming numerous short-range contacts with other biopolymers concurrently	Facilitating component aggregation, hydroxyl and hydrocarbon groups support hydrogen bonding and hydrophobic interactions with the remaining components
Humic substance	Mainly on the periphery of clusters	Impeded the smooth aggregation of clusters, dictated EPS surface properties, formed hydrophobic pockets with LIPs on cluster surface
Lipid	Distributed between central and peripheral components, interacting with hydrophobic groups	Acted as hydrophobic bridges for hydrophobic molecules, increased cluster hydrophobic surface area
Small molecule acid	Mainly on the periphery with a wide range of motion	Influencing the surface properties of clusters and facilitating resource translocation
Metal ions	Distributed inside the clusters, bridged the negatively charged groups	Promoted cross-linking between biopolymers, reduced repulsion among negatively charged groups, enhanced cluster stability

for faithful modeling of realistic EPS, permitting a rigorous molecular interpretation of complex mesoscopic observations. This is especially important in relation to EPS molecular structure and biopolymer distribution observed through biofilm matrix biology investigations using a variety of in situ imaging and chemical characterizations (43–45). Microscopic characterization methods such as fluorescence in situ hybridization, atomic force microscopy, and quartz crystal microbalance with dissipation can be used to determine the distribution of components, surface properties, and structural strength of EPS. This facilitates the establishment of a quantitative relationship between simulation results and actual properties, enhancing the accuracy of model predictions (46–48). Although there are still computational and analytical challenges in matching realistic temporal and spatial scales while not losing molecular specificity in EPS models, this study provided a strategy to extract statistically insightful information on EPS aggregation process and component interactions; broader conformational dynamics can be accessed by combining model derivation (e.g. Markov state models, etc.) based on these trajectories and intermediate states (49, 50). In addition, the presented modeling strategy holds considerable potential for advancing the capture of complex molecular features of various extracellular matrixes; more valuable details of biopolymer interactions can be described by enforcing the connection between model iterations and experiments. Further construction of EPS models from multiple different sources and EPS–cell membrane interaction models can reveal the complex interfacial behavior and reaction processes in wastewater treatment processes.

Materials and methods

EPS extraction

Fresh AAS and ADS were collected from the same operating system of a wastewater treatment plant located in Beijing, China, and the basic properties of AAS and ADS are provided in Table S11. EPS was extracted by cation exchange resin technique because of its low cellular damage and easy separation (51). The detailed procedures for EPS extraction and content analysis are provided in Text S1 (Supplementary Information).

Key components separation and structural characterization

The methods of protein isolation from EPS were modified on the basis of trichloroacetic acid sedimentation. PS was isolated and purified using the precipitation method with ethanol. HSs were purified according to the methods provided by the International Humic Substances Society. The detailed separation procedures for each component are described in Text S2. The MW of the separated components was then analyzed by an Agilent LC pump Series 1220 (CA-1220; Agilent Co., USA) equipped with a HPLC-SEC. Proteins were analyzed by 4D label-free-based mass spectrometry proteomics, and iBAQ algorithm was used to find the abundant proteins in the samples (52). Details for the procedures for proteomics analysis and abundance assessment are provided in Text S4. PS molecular structure was resolved by monosaccharide composition analysis, partial acid hydrolysis analysis, and methylation analysis, and details for the methods are given in Text S5. Elemental analysis and NMR spectroscopy were employed to characterize HS, and additional details of the method are given in Text S6.

Biopolymer models construction

The structure of identified proteins was predicted utilizing SWISS-MODEL and AlphaFold 2.3 based on the amino acid sequences collected from UniProt database (53, 54). The highest ranking predicted model determined by Global Model Quality Estimate and predicted local distance difference test score was selected. Meanwhile, PE chain models were constructed based on high-intensity PE sequences detected in proteomic analysis. The PS models and molecular force field topology were generated using GLYCAM-Web (http://glycam.org). VSOMM2 (https://somm.boku.ac.at/) was used to generate the theoretical models of HS molecules, and the characterization data were input through the advanced model to complete the model calculations (55). The resulting model was processed and structurally optimized by Avogadro 1.2 (56). LIP molecules were screened by the fourier transform ion cyclotron resonance mass spectrometry analysis of extracellular organic matter of the same sludge samples in our other studies. The structure of selected biomolecules was identified via LIPID MAPS (http://www.lipidmaps.org/). Monophosphate nucleotides consisting of adenosine, cytidine, thymidine, and guanosine were chosen as the model for NAs. Serine, tryptophan, and phenylalanine were identified as FAA components in the EPS model based on the analysis of FAA (Table S12). NA and FAA formed the SMA component of the EPS cluster model.

MD details

All the simulations were performed using GROMACS (2020.6) program in TIP3P H2O model with the periodic boundary conditions

(57). The Amber14SB force field was used for the protein and NA molecules, and the force field for PS, HS, and LIP was obtained using AmberTools23 (58). The additional details on the computation and analysis of trajectories are given in Text S7.

Supplementary Material

Supplementary material is available at *PNAS Nexus* online.

Funding

This work was supported by the National Natural Science Foundation of China (nos. 52388101 and 52122010).

Author Contributions

S.P. was involved in conceptualization, methodology, formal analysis, date curation, investigation, software, visualization, and writing—original draft. Z.W. was involved in investigation, formal analysis, and writing—revising and editing. J.A. was involved in date curation and writing—revising and polishing. L.L. was involved in methodology and date curation. H.Z., Y.Z., and D.W. were involved in investigation. G.L. was involved in validation. B.-J.N. was involved in conceptualization and writing—revising and editing. G.-P.S. and C.H. were involved in resources. W.Z. was involved in conceptualization, methodology, validation, resources, writing—review and editing, and supervision.

Data Availability

All data are included in the article and Supplementary material.

References

1 Nagwekar PR. 2014. Removal of organic matter from wastewater by activated sludge process–review. *Int J Sci Eng Technol Res*. 3(5):1260–1263.
2 Yu H-Q. 2020. Molecular insights into extracellular polymeric substances in activated sludge. *Environ Sci Technol*. 54(13):7742–7750.
3 Xiao R, Zheng Y. 2016. Overview of microalgal extracellular polymeric substances (EPS) and their applications. *Biotechnol Adv*. 34(7):1225–1244.
4 Guo W-Q, Yang S-S, Xiang W-S, Wang X-J, Ren N-Q. 2013. Minimization of excess sludge production by in-situ activated sludge treatment processes—a comprehensive review. *Biotechnol Adv*. 31(8):1386–1396.
5 Hao X, Chen Q, van Loosdrecht MC, Li J, Jiang H. 2020. Sustainable disposal of excess sludge: incineration without anaerobic digestion. *Water Res*. 170:115298.
6 Flemming H-C, Wingender J. 2010. The biofilm matrix. *Nat Rev Microbiol*. 8(9):623–633.
7 Yuan DQ, Wang YL, Feng J. 2014. Contribution of stratified extracellular polymeric substances to the gel-like and fractal structures of activated sludge. *Water Res*. 56:56–65.
8 Flemming H-C, *et al.* 2016. Biofilms: an emergent form of bacterial life. *Nat Rev Microbiol*. 14(9):563–575.
9 Zhang W, Dai X, Dong B, Dai L. 2020. New insights into the effect of sludge proteins on the hydrophilic/hydrophobic properties that improve sludge dewaterability during anaerobic digestion. *Water Res*. 173:115503.
10 Tang Y, Dai X, Dong B, Guo Y, Dai L. 2020. Humification in extracellular polymeric substances (EPS) dominates methane release and EPS reconstruction during the sludge stabilization of high-solid anaerobic digestion. *Water Res*. 175:115686.
11 Sheng GP, Yu HQ, Li XY. 2010. Extracellular polymeric substances (EPS) of microbial aggregates in biological wastewater treatment systems: a review. *Biotechnol Adv*. 28(6):882–894.
12 Lv L, *et al.* 2023. Regulation of extracellular polymers based on quorum sensing in wastewater biological treatment from mechanisms to applications: a critical review. *Water Res*. 250:121057.
13 Liu L, Huang Q, Qin B. 2018. Characteristics and roles of Microcystis extracellular polymeric substances (EPS) in cyanobacterial blooms: a short review. *J Freshwater Ecol*. 33(1):183–193.
14 Quijano G, Arcila JS, Buitrón G. 2017. Microalgal-bacterial aggregates: applications and perspectives for wastewater treatment. *Biotechnol Adv*. 35(6):772–781.
15 Nguyen TDP, *et al.* 2019. Bioflocculation formation of microalgae-bacteria in enhancing microalgae harvesting and nutrient removal from wastewater effluent. *Bioresour Technol*. 272:34–39.
16 Peng S, Hu A, Ai J, Zhang W, Wang D. 2021. Changes in molecular structure of extracellular polymeric substances (EPS) with temperature in relation to sludge macro-physical properties. *Water Res*. 201:117316.
17 Boleij M, Pabst M, Neu TR, Van Loosdrecht MC, Lin Y. 2018. Identification of glycoproteins isolated from extracellular polymeric substances of full-scale anammox granular sludge. *Environ Sci Technol*. 52(22):13127–13135.
18 Seviour T, Yuan Z, van Loosdrecht MC, Lin Y. 2012. Aerobic sludge granulation: a tale of two polysaccharides? *Water Res*. 46(15):4803–4813.
19 Felz S, Neu TR, van Loosdrecht MCM, Lin Y. 2020. Aerobic granular sludge contains hyaluronic acid-like and sulfated glycosaminoglycans-like polymers. *Pergamon*. 169:115291.
20 Boleij M, Seviour T, Wong LL, van Loosdrecht MCM, Lin Y. 2019. Solubilization and characterization of extracellular proteins from anammox granular sludge. *Water Res*. 164:114952.
21 Zhang P, Feng B, Chen Y-P, Dai Y-Z, Guo J-S. 2019. In situ characterizations for EPS-involved microprocesses in biological wastewater treatment systems. *Crit Rev Environ Sci Technol*. 49(11):917–946.
22 Chen W, Qian C, Zhou K-G, Yu H-Q. 2018. Molecular spectroscopic characterization of membrane fouling: a critical review. *Chem*. 4(7):1492–1509.
23 Neu TR, Kuhlicke U. 2017. Fluorescence lectin bar-coding of glycoconjugates in the extracellular matrix of biofilm and bioaggregate forming microorganisms. *Microorganisms*. 5(1):5.
24 Seviour T, *et al.* 2019. Extracellular polymeric substances of biofilms: suffering from an identity crisis. *Water Res*. 151:1–7.
25 Flemming HC, *et al.* 2023. The biofilm matrix: multitasking in a shared space. *Nat Rev Microbiol*. 21(2):70–86.
26 Devarajan D, *et al.* 2020. Molecular dynamics simulation of the structures, dynamics, and aggregation of dissolved organic matter. *Environ Sci Technol*. 54(21):13527–13537.
27 Xu G, Wang H, Sun W. 2018. Molecular dynamics study of rejuvenator effect on RAP binder: diffusion behavior and molecular structure. *Constr Build Mater*. 158:1046–1054.
28 Weng J, Yang M, Wang W, Xu X, Tian Z. 2020. Revealing thermodynamics and kinetics of lipid self-assembly by Markov state model analysis. *J Am Chem Soc*. 142(51):21344–21352.
29 Liu J, *et al.* 2019. Actinia-like multifunctional nanocoagulant for single-step removal of water contaminants. *Nat Nanotechnol*. 14(1):64–71.
30 Liu Y, *et al.* 2022. Molecular dynamics simulation study of covalently bound hybrid coagulants (CBHyC): molecular structure and coagulation mechanisms. *Chemosphere*. 307(Pt 3):135863.

31 Peng S, *et al.* 2024. Molecular dynamic modeling of EPS and inorganic/organic flocculants during sludge dual conditioning. *Sci Total Environ*. 906:167719.
32 Liu Y, Liu X, Liu L. 2023. Molecular dynamics simulation of the aggregation of extracellular polymeric substance. In: *E3S Web of Conferences*. Vol. 406. EDP Science: p. 01009.
33 Peng S, *et al.* 2023. Aggregation and construction mechanisms of microbial extracellular polymeric substances with the presence of different multivalent cations: molecular dynamic simulation and experimental verification. *Water Res*. 232:119675.
34 Kaur S, Kulharia M. 2017. Insights from the molecular dynamics simulation of BcsD subunit from K. xylinus. *Bioinformation*. 13(11): 376–379.
35 Li G-F, *et al.* 2021. Molecular insight into the binding property and mechanism of sulfamethoxazole to extracellular proteins of anammox sludge. *Environ Sci Technol*. 55(24):16627–16635.
36 Böhning J, *et al.* 2022. Donor-strand exchange drives assembly of the TasA scaffold in Bacillus subtilis biofilms. *Nat Commun*. 13(1):7082.
37 Basak S, *et al.* 2019. Networks of electrostatic and hydrophobic interactions modulate the complex folding free energy surface of a designed βα protein. *Proc Natl Acad Sci U S A*. 116(14):6806–6811.
38 Chen S-J, Dill KA. 2000. RNA folding energy landscapes. *Proc Natl Acad Sci U S A*. 97(2):646–651.
39 Ghosh P, Mondal J, Ben-Jacob E, Levine H. 2015. Mechanically-driven phase separation in a growing bacterial colony. *Proc Natl Acad Sci U S A*. 112(17):E2166–E2173.
40 Aldeek F, *et al.* 2013. Patterned hydrophobic domains in the exopolymer matrix of Shewanella oneidensis MR-1 biofilms. *Appl Environ Microbiol*. 79(4):1400–1402.
41 Wang S, *et al.* 2020. The branched chains and branching degree of exopolysaccharides affecting the stability of anammox granular sludge. *Water Res*. 178:115818.
42 Zhou H, *et al.* 2024. Regional heterogeneity of sustainable wastewater sludge management in China. *Resour Conserv Recy*. 209:107755.
43 Laughlin ST, Bertozzi CR. 2009. Imaging the glycome. *Proc Natl Acad Sci U S A*. 106(1):12–17.
44 Geva-Zatorsky N, *et al.* 2015. In vivo imaging and tracking of host–microbiota interactions via metabolic labeling of gut anaerobic bacteria. *Nat Med*. 21(9):1091–1100.
45 Liu X-Y, *et al.* 2019. Spatiotemporal organization of biofilm matrix revealed by confocal Raman mapping integrated with non-negative matrix factorization analysis. *Anal Chem*. 92(1): 707–715.
46 Wang Z, van Loosdrecht MC, Saikaly PE. 2017. Gradual adaptation to salt and dissolved oxygen: strategies to minimize adverse effect of salinity on aerobic granular sludge. *Water Res*. 124: 702–712.
47 Lu Q, *et al.* 2023. Molecular insights into the interaction mechanism underlying the aggregation of humic acid and its adsorption on clay minerals. *Environ Sci Technol*. 57(24): 9032–9042.
48 AbuKhadra D, *et al.* 2024. The effect of temperature on fouling in anaerobic membrane bioreactor: SMP-and EPS-membrane interactions. *Water Res*. 260:121867.
49 Husic BE, Pande VS. 2018. Markov state models: from an art to a science. *J Am Chem Soc*. 140(7):2386–2396.
50 Korevaar PA, *et al.* 2012. Pathway complexity in supramolecular polymerization. *Nature*. 481(7382):492–496.
51 Ai J, *et al.* 2021. Understanding synergistic mechanisms of ferrous iron activated sulfite oxidation and organic polymer flocculation for enhancing wastewater sludge dewaterability. *Water Res*. 189: 116652.
52 Shin J-B, *et al.* 2013. Molecular architecture of the chick vestibular hair bundle. *Nat Neurosci*. 16(3):365–374.
53 Bordoli L, *et al.* 2009. Protein structure homology modeling using SWISS-MODEL workspace. *Nat Protoc*. 4(1):1–13.
54 Jumper J, *et al.* 2021. Highly accurate protein structure prediction with AlphaFold. *Nature*. 596(7873):583–589.
55 Petrov D, Tunega D, Gerzabek MH, Oostenbrink C. 2017. Molecular dynamics simulations of the standard leonardite humic acid: microscopic analysis of the structure and dynamics. *Environ Sci Technol*. 51(10):5414–5424.
56 Hanwell MD, *et al.* 2012. Avogadro: an advanced semantic chemical editor, visualization, and analysis platform. *J Cheminform*. 4:17.
57 Spoel VD. GROMACS 2020 Source code. *Zenodo*. https://doi.org/10.5281/zenodo.3562494 Date of deposit 3 March 2020.
58 Case DA, *et al.* 2023. AmberTools. *J Chem Inf Model*. 63(20): 6183–6191.